



Understanding the distribution of natural wax in starch–wax films using synchrotron-based FTIR (S-FTIR)



Delina Muscat^a, Mark J. Tobin^b, Qipeng Guo^c, Benu Adhikari^{a,d,*}

^a School of Health Sciences, University of Ballarat, VIC 3353, Australia

^b IR Beamline, Australian Synchrotron, Clayton, VIC 3168, Australia

^c Institute for Frontier Materials, Deakin University, Waurn Ponds, VIC 3219, Australia

^d School of Applied Sciences, RMIT University, City Campus, Melbourne, VIC 3001, Australia

ARTICLE INFO

Article history:

Received 21 June 2013

Received in revised form 10 October 2013

Accepted 2 November 2013

Available online 13 November 2013

Keywords:

High amylose starch

Films

Natural wax

Synchrotron-FTIR

Surface hydrophobicity

ABSTRACT

High amylose starch–glycerol (HAG) films were produced incorporating beeswax, candelilla wax and carnauba wax in the presence and absence of Tween-80 in order to determine the distribution of wax in the films during the film formation process. The distribution of these waxes within the film was studied using Synchrotron based Fourier Transform Infrared Spectroscopy (S-FTIR) which provided 2D mapping along the thickness of the film. The incorporation of 5% and 10% wax in HAG films produced randomly distributed wax or wax-rich domains, respectively, within these films. Consequently, the addition of these waxes to HAG increased the surface roughness and hydrophobicity of these films. The addition of Tween-80 caused variations in wax-rich bands within the films. The HAG + carnauba wax + Tween-80 films exhibited domed wax-rich domains displayed with high integrated CH₂ absorption value at the interior of the films, rougher surface and higher contact angle values than the other films. The S-FTIR 2D images indicated that the distribution of wax in starch–wax films correlated with the roughness and hydrophobicity of the starch–wax films.

© 2013 Elsevier Ltd. All rights reserved.

1. Introduction

With the continuous depletion of fossil fuel resources and the accelerating environmental problem of disposing of petroleum-based plastics, there is an increasing research interest in developing biodegradable packaging from renewable natural resources (Rhim & Ng, 2007). Such renewable resources include polysaccharides and lipids (Bourliew, Guillard, Vallès-Pamiès, & Gontard, 2008). If stand-alone or primary packaging can be developed by a judicious combination of polysaccharides and lipids they can become an alternative to the synthetic polymer based packaging (Rhim & Shellhammer, 2005; Zhang & Han, 2006).

Although starch has been used to develop flexible packaging films, the inherent characteristics of starch such as sensitivity to water, brittleness and relatively poor flexibility have limited the utilization of its full potential. Lipids are incorporated in the matrix of starch films to improve the water barriers properties and water repelling properties in starch-based films. This is because lipids bring in hydrophobicity and starch–lipid films possess low surface

energy (Han & Gennadios, 2005). The oil-in-water (O/W) emulsion is one of the commonly used methods in producing starch–lipid composite films. In these starch–lipid composite films the lipid component is responsible for providing a better water barrier, while the starch provides a selective barrier to oxygen and carbon dioxide and the necessary supporting backbone (Perez-Gago & Krochta, 2005).

The O/W emulsion method is a one-step technique where the lipid is dispersed into the gelatinized starch solution prior to film casting. During drying of this starch–lipid emulsion, two types of films having quite different physical structures can be formed. One type of film is produced when the continuous phase (i.e. gelatinized starch solution) cannot stabilize the emulsion therefore phase separation occurs causing the lipid to migrate to the surface of film forming a lipid-rich surface layer (Perez-Gago & Krochta, 2005). The other type of film formed during drying is when the lipid material is randomly or uniformly dispersed throughout the gelatinized starch continuous phase.

With the recent progress in infrared (IR) spectroscopy, which includes combination of IR spectroscopy with microscopy, has improved the spectral quality and reproducibility of infrared measurements in small or thin film samples. The advent of a synchrotron light source has enabled researchers to obtain high quality infrared spectra at diffraction-limited spot sizes using commercial infrared microscope systems. The synchrotron is of great advantage

* Corresponding author at: School of Health Sciences, University of Ballarat, VIC 3353, Australia. Tel.: +61 3 53279249; fax: +61 3 53279840.

E-mail addresses: b.adhikari@ballarat.edu.au,
benu.adhikari@rmit.edu.au (B. Adhikari).

when ultra-high spatial resolution is required near the diffraction limit of 3–10 μm (Holman et al., 2002; McNaughton, 2005; Yu, 2004) since the brightness of the synchrotron infrared source allows more photons to be detected in a given interval (Dumas, Sockalingum, & Sule-Suso, 2007). Synchrotron-based IR imaging has made it possible to obtain the detailed spatial distribution of chemical compounds in materials by the generation of chemical images at a rapid data acquisition (Ali, Das, Lu, Kundapur, & May, 2011).

All biopolymers have unique molecular chemical-structural features which contribute to their own unique IR spectrum. Lipids contain both carbonyl $\text{C}=\text{O}$ ester as well as CH_2 and CH_3 functional groups. The unique IR spectral features in lipids are observed at 1738 cm^{-1} ($\text{C}=\text{O}$ stretch, i.e. ester carbonyl functional group, $-\text{COOH}$), 1470 cm^{-1} (CH bending), 2961 cm^{-1} (antisymmetric CH_3 stretching), 2925 cm^{-1} (antisymmetric CH_2 stretching), 2871 cm^{-1} (symmetric CH_3 stretching), and 2853 cm^{-1} (symmetric CH_2 stretching) (Yu, 2004, 2012). Then the IR spectral features of corn starch consists of its major structure between 3000 and 3600 cm^{-1} due to OH stretching (Coates, 2000; Zhang & Han, 2006). The sharp peak at 2924 cm^{-1} is characteristic of $\text{C}-\text{H}$ stretching (CH_2) (Park, Im, Kim, & Kim, 2000). The peak occurring at 1641 cm^{-1} is associated with the tightly bound water present in the starch (Zhang & Han, 2006) due to the hygroscopic nature of starch. The peaks at 1409 and 1433 cm^{-1} are related to the $\text{C}-\text{H}$ bending of CH_2 . Peaks at 1240, 1299, and 1333 cm^{-1} are associated to $\text{O}-\text{H}$ bending due to the primary or secondary alcohols (Coates, 2000). These characteristic IR spectra of the starch and lipid can assist in characterizing a composite film by the evaluation of interactions between these two components in starch–lipid composite films.

The synchrotron-based Fourier transform infrared spectroscopy (S-FTIR) is capable of providing important information such as distribution of the chemical constituents and functional groups of wax within the starch–wax composite films. This information helps to gain fundamental understanding of how chemical functional components (for example that of wax) are distributed at the micron scale in the films produced through O/W emulsion method (Yu, 2004). The chemical imaging capability of S-FTIR simultaneously provides both the morphological and chemical information within such composite films.

To the best of our knowledge, the chemical imaging capability of S-FTIR has not been applied to investigate the structural feature and the distribution of natural wax in high amylose starch–glycerol (HAG) films produced using the O/W emulsion method. The S-FTIR is also capable of providing important insights on the structural–chemical features created due to the interactions among the components (wax, HAG matrix, water and the emulsifier) of the composite films.

In this context, the objective of this study was to apply the S-FTIR 2D mapping to determine the distribution of wax and starch within the thin HAG–wax films produced through the (O/W) emulsion method, i.e. to observe whether or not a uniform wax layer can be formed on top of the starch matrix. The information obtained through S-FTIR 2D imaging was compared with the contact angle data of the film to correlate between the distribution of wax on the film surface with the measured film hydrophobicity (through contact angle) and its surface topography.

2. Materials and methods

2.1. Materials

High amylose (HA) corn starch (Gelose 80) containing 70–80% (w/w) amylose was purchased through Penfolds (Australia) and constituted the continuous matrix of the starch–wax films. Glycerol

(G) was used as a plasticizer and was purchased from Consolidated Chemical Company (Melbourne, Australia). Tween-80 was used as an emulsifier and was purchased from Sigma Aldrich (Australia). Three natural waxes, i.e. beeswax (BW), candelilla wax (CL) and carnauba wax (CB), were purchased from New Directions Aromatics Inc. (Australia). The Certificate of Analysis of these waxes was provided by this company. All the materials were used as received and the moisture content of the raw materials was measured and was compensated for while preparing the slurry mixture before gelatinization.

2.2. Methods

2.2.1. Suspension preparation, film casting and conditioning

The high amylose starch (HA) and glycerol (G) were added to distilled water maintaining a total solid concentration of 5% (w/w). The HA:G dry solid ratio of 80:20 was maintained to produce good flexible films as reported in our previous study (Muscat, Adhikari, Adhikari, & Chaudhary, 2012).

The HAG suspension was gelatinized using a high temperature–high pressure laboratory autoclave (Amar Equipment Company, Mumbai, India). The HAG suspension was gelatinized at 140°C using 500 rpm agitator speed. The suspension was held for 30 min at 140°C before cooling down to below 100°C . While maintaining a temperature above 85°C by using a hot plate (Framo Geratechnik, Germany), Tween-80 (20% w/w) was added to the fully gelatinized HAG dispersion and thoroughly stirred. In producing the HAG–wax film using the (O/W) emulsion method, the dispersion was kept heated above 85°C before the molten waxes were added. The beeswax (BW), candelilla wax (CL) and carnauba wax (CB) were added individually at two different concentrations of 5% (w/w) and 10% (w/w) with and without Tween-80. To ensure a thorough mixing of molten wax droplets within the HAG dispersion, coarse homogenization was carried out using a high-shear mixer (Ultra-Turrax, Model T25, IKA-Works, USA) at 15,000 rpm for 3 min. Further intense homogenization was carried out at 22,000 rpm for 5 min using the same homogenizer.

The films were produced by casting method by syringing 10 mL of the suspension into plastic polystyrene dishes having 90 mm diameter. Films were dried overnight at $20 \pm 1^\circ\text{C}$, in an air conditioned room. These films were stored in a desiccator containing magnesium nitrate (52.9% RH ($a_w = 0.529$)) at $20 \pm 1^\circ\text{C}$ for at least 48 h for conditioning before further analysis.

2.2.2. Interaction among the film components

To identify the specific spectral “signatures” of these natural waxes (BW, CL and CB) solid samples of each wax were analyzed by FTIR spectroscopy. The specific spectral “signatures” of these natural waxes were determined by using a universal attenuated total reflectance (UATR) FTIR spectrometer (Perkin Elmer, FrontierTM, USA) having diamond coated zinc selenide crystal probe (reflection plate with pressure arm). Perkin-Elmer spectrum software (version 6.3.4) was used for FTIR analysis. The spectra were obtained between 1100 cm^{-1} and 4000 cm^{-1} wavenumbers at 4 cm^{-1} step.

2.2.3. Film structure analysis

Film surface topography was examined by using scanning electron microscopy (SEM, JEOL-JSM 6300, Japan). Films were mounted onto a double sided adhesive carbon tape set on aluminium stubs, which were gold coated under vacuum. The gold coated samples were analyzed at 5 kV, $4500\times$ magnification and at an angle of 25° to the surface in order to allow better observation of the cross section of the film.

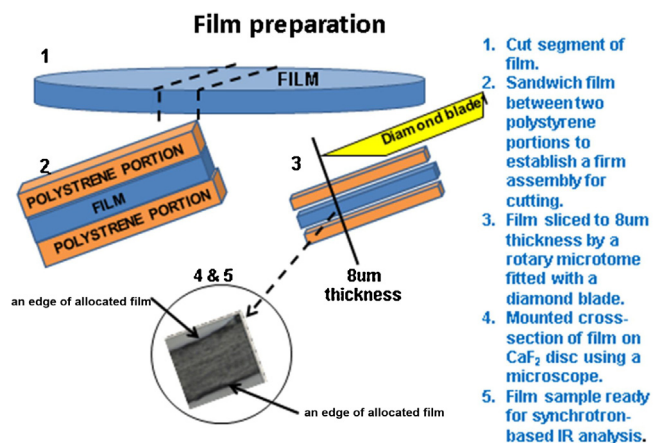


Fig. 1. Schematic diagram of film preparation for synchrotron-based IR analysis.

2.2.4. Contact angle

The contact angle (CA) is the most common measure of wettability or surface hydrophobicity. The static sessile drop method where the angle formed at triple solid–liquid–air was used to determine the contact angle of the HAG + wax + Tween-80 films. The contact angle apparatus used has been reported in our previous study (Muscat, Adhikari, McKnight, Gio, & Adhikari, 2013). It consisted of a microscope optical system (Zeiss, Carl Zeiss Microscopy GmbH, Germany) connected to a high resolution digital camera (EOS 60D, Canon, USA). Software to capture the digital image was part of the camera hardware and images were captured in a personal computer. A horizontal beam held the microscope parallel to the surface and was positioned on a three-axis moving platform. To provide lighting, a bank of LEDs was mounted behind the sample holder with a white background.

The film was mounted to a stainless steel block with double sided tape. The drop (7 μL) of Milli-Q water was carefully placed on the horizontal surface of the film with the aid of an auto pipette (Finnpipette, 0.5–10 μL). The CA values were determined using ImageJ program (Rasband, 2012) with a plug-in program for contact angle measurement (Brugnara, 2006). The plug-in program fits the profile of the drop using an edge detection algorithm to find the drop edge (Williams et al., 2010) and calculates the contact angle using the sphere approximation or the ellipse approximation. In our study, the both BestFits selection gave consistent results for contact angles >30° and the sphere selection was used for drops with contact angles <30° (Brugnara, 2006; Williams et al., 2010). The reported contact angle values are the mean value of five measurements taken at least four different positions on the film.

2.2.5. Preparation of films for S-FTIR microspectroscopy

A section of the film sample was inserted between two polystyrene portions to establish a firm assembly for cutting (Fig. 1). The embedded film sample was cut into thin cross-sections along the film thickness (ca. 8 μm thick) using a rotary microtome (4060RE, Triangle Biomedical Sciences, Inc., USA) at the Australian Synchrotron (Clayton, Victoria) 24 h prior to its analysis using S-FTIR. The cross-sections were mounted onto CaF₂ windows (size: 13 mm × 1 mm disk; Cymat Limited, UK) for transmission mode S-FTIR analysis.

2.2.6. Molecular spectral data analysis and imaging of molecular chemistry

The S-FTIR measurements were performed on the FTIR beamline at the Australian Synchrotron (Clayton, Victoria). Spectra were collected with a Bruker Hyperion 2000 IR microscope (Bruker Optik GmbH, Ettlingen, Germany) equipped with a liquid nitrogen cooled

HgCdTe (MCT) detector with a 36× IR objective. The Hyperion 2000 microscope was coupled to a Bruker Vertex 80 spectrometer. Spectral maps and line scans were collected in transmission by scanning the computer-controlled microscope stage at an aperture of 5 μm × 5 μm, and an x–y spatial step size of 2 μm.

The spectra data of the films were collected in the mid-IR range 4000–1100 cm^{−1} using a CaF₂ window (Miller, 2002), at a resolution of 4 cm^{−1} with 64 scans co-added. The stage control, data collection and the background correction of the spectra were performed using Opus 6.5 (Bruker, Optik GmbH, Ettlingen, Germany) software version 2.0. Data were saved as Opus Spectrum files for single spectra and Opus Multiple files for 2D IR map files. Opus Multiple files contain all spectral and x–y spatial information for a two dimensional grid map as well as the captured images. Opus 7.0 (Bruker, Optik GmbH, Ettlingen, Germany) software was equipped with video mapping capability and it was used to generate and analyze 2D absorbance maps and the data were converted into 3D chemical maps.

2.2.7. Selection of an IR band in natural waxes to quantify wax distribution in the studied films

Spectra of the natural waxes were analyzed by the UATR FTIR spectrometer to identify functional groups present in these waxes (Fig. 2). The most intense vibrations in the infrared spectra of lipid systems are the CH₂ stretching vibration regions. The CH₂ antisymmetric and symmetric stretching modes observed at 2916 cm^{−1} and 2848 cm^{−1}, respectively, are generally the strongest bands in the IR spectra of lipids (Stuart, 2004). These IR bands are associated with the presence of alkanes. The IR spectra of both HAG films and Tween-80 are also presented in Fig. 2 for comparison. Furthermore, it can be seen from Fig. 2 that the IR absorption peak at 2848 cm^{−1} is only observed in the IR spectra of natural waxes and not in that of HAG. Plotting the integrated area of the antisymmetric CH₂ peak, as a function of position across each sample, it was possible to assess the wax distribution in each microtomed section. To generate infrared absorbance maps, the integrated area of the CH₂ antisymmetric peak at 2848 cm^{−1} was calculated for each pixel within each data set, with the integration calculated above a baseline between two points on the spectral curve at 2860 cm^{−1} and 2830 cm^{−1}. No additional baseline correction to the spectra was undertaken prior to calculation of the integrals. It can also be seen from Fig. 2 that the IR spectrum of Tween-80 also shows characteristic IR absorption peaks at 2916 cm^{−1}, 2848 cm^{−1} and 1736 cm^{−1} which is similar to the characteristic peaks in the spectra of natural waxes. Therefore, the chemical images and chemical intensity scale of HAG + wax + Tween-80 films at 2848 cm^{−1} (Figs. 6 and 7) would be influenced due to the presence of Tween-80 and wax.

The chemical intensity scale displays a range of colours from blue to pink or white to make it easier to interpret the distribution of wax within the films under the peak centred at 2848 cm^{−1} showing CH₂ stretching of the wax. As shown in Figs. 3–7 the blue suggests the absence of wax, whereas pink and/or white denotes the presence of wax at a high concentration. From the chemical intensity scale one is able to understand and reveal the pattern of wax distribution within these films.

2.2.8. Statistical analysis

Statistical analysis was performed using two-tailed Student's *t*-tests at 95% confidence level using Minitab 15 software (Minitab, Australia). A *p* value ≤0.05 was set for statistical significance.

3. Results and discussion

The S-FTIR technique could be used in order to reveal the distribution of natural waxes within the HAG + wax and

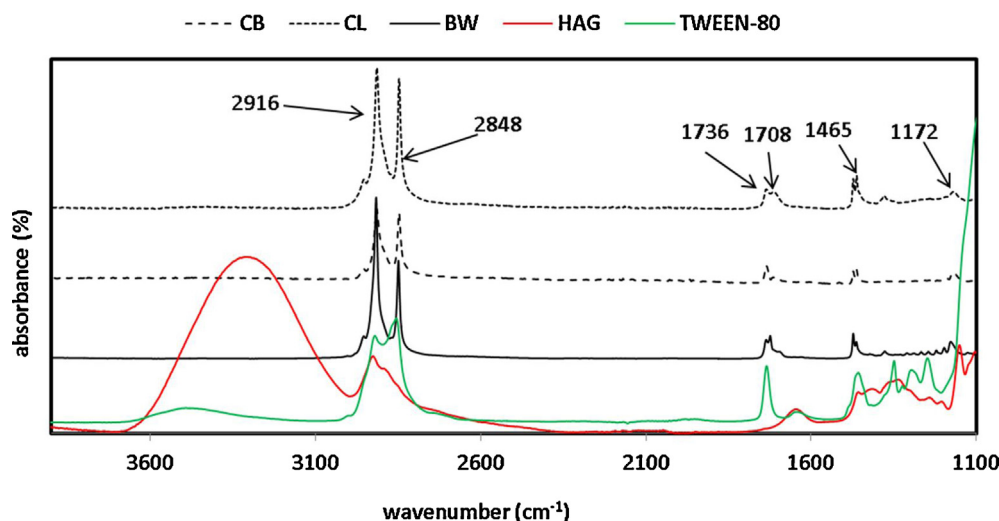


Fig. 2. Typical spectra of natural wax (beeswax (BW), candelilla wax (CL), carnauba wax (CB)), high amylose and glycerol (HAG) film and Tween-80 in the IR range. The natural waxes have characteristic C–H stretching vibration at 2916 cm^{-1} and 2848 cm^{-1} , C=O stretching (i.e. ester carbonyl functional group) at 1736 cm^{-1} and 1708 cm^{-1} , C–H bending at 1465 cm^{-1} and C–O stretching at 1172 cm^{-1} . The HAG and Tween-80 spectra are displayed to identify similar peaks to the waxes spectra. This figure indicates that the wavenumbers 2848 cm^{-1} and 1736 cm^{-1} are unique characteristic to waxes and Tween-80.

HAG + wax + Tween-80 films. As discussed above, the spatial distribution and S-FTIR intensity of the functional group of lipid (wax) can be used to determine the distribution of the natural wax in the film. S-FTIR provides the mapping of specific functional groups of biopolymers including lipids. The chemical images of wax components from the cross-section of the HAG, HAG + wax 5%, HAG + wax 10%, HAG + wax 5% + Tween-80 and HAG + wax 10% + Tween-80 films are shown in Figs. 3–7, respectively. Figs. 3–7 show the following 3 important aspects in starch–wax films: (1) chemical map with colour codes to indicate presence of wax and/or Tween-80; (2) CH_2 absorbance intensity scale; (3) CH_2 distribution profiles of wax across the thickness of the film at the 2848 cm^{-1} wave number.

The HAG film was used as a control, as the specific functional group which exhibits the IR absorption at 2848 cm^{-1} is not present in the spectrum of this film (Fig. 2). The chemical map shown in Fig. 3 clearly indicates that there was no trace of wax in HAG film as expected.

3.1. The distribution of wax in HAG + wax films

The addition of 5% BW, CL and CB to HAG film matrix (Fig. 4) revealed that each wax was fairly evenly distributed within these films as can be seen from the CH_2 distribution profiles. The variation in CH_2 absorbance intensity within each of these samples was less than 50% with HAG + 5% BW showing variation in the CH_2 peak integrated area from 4.6 (dark pink shading) to 6.2 (light pink shading) and HAG + 5% CL showing variation from 5.2 (orange shading) to 7.6 (pink shading). The map of HAG + 5% CB showed that at most locations the integrated CH_2 absorbance ranged from 0.75 (green shading) to 1.10 (red shading). A single higher concentration domain was observed in the HAG + 5% CB sample with an integrated absorbance value of approximately 1.35. This observation suggests that at 5% concentration all of these waxes crystallized at an earlier stage of the drying process within the composite films, i.e. before the completion of the film formation. This is due to the fact that the temperature of the cast emulsion decreased to the

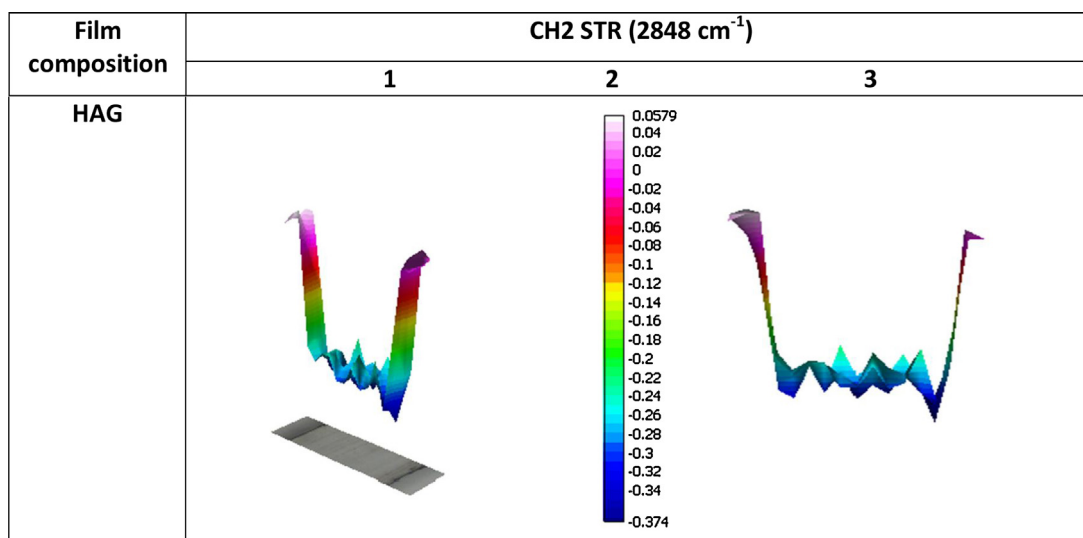


Fig. 3. The functional-group image of wax component within a cross-section of the HAG film. (1) Chemical map with colour codes to indicate presence of wax and Tween-80; (2) CH_2 absorbance intensity scale; (3) CH_2 distribution profiles of wax across the thickness of the film. Area under peak centred at 2848 cm^{-1} showing CH_2 stretching, lipid distribution and intensity. (For interpretation of the references to colour in this figure legend, the reader is referred to the web version of this article.)

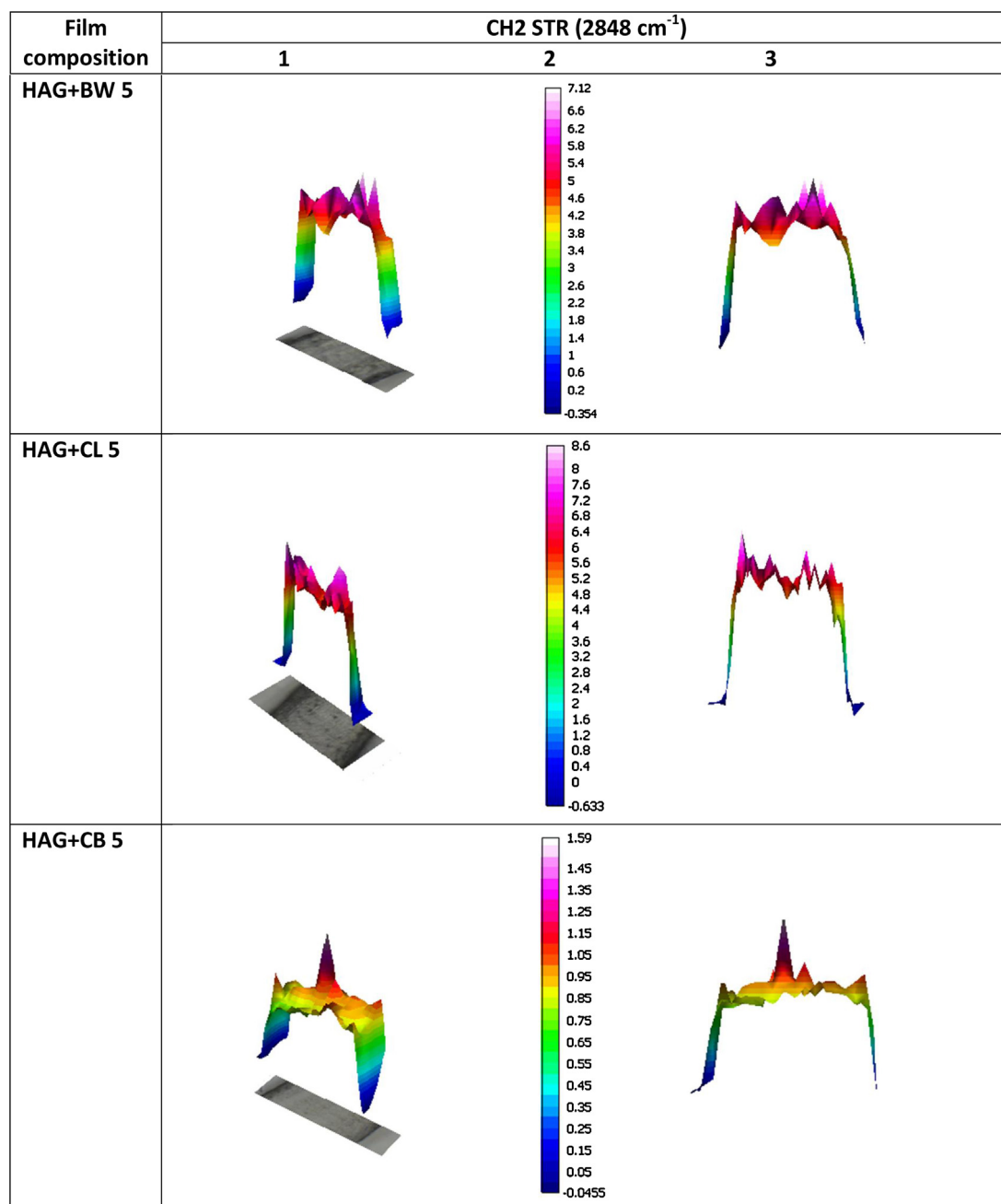


Fig. 4. The functional-group images of wax component within a cross-section of the HAG + 5% wax films. (1) Chemical map with colour codes to indicate presence of wax and/or Tween-80; (2) CH₂ absorbance intensity scale; (3) CH₂ distribution profiles of wax across the thickness of the film. Area under peaks centred at 2848 cm⁻¹ showing CH₂ stretching, lipid distribution and intensity. (For interpretation of the references to colour in this figure legend, the reader is referred to the web version of this article.)

ambient temperature (20 °C) soon after the drying started which facilitated the random crystallization of the wax. The melting points of beewax, candelilla wax and carnauba wax are 62–64 °C, 66–71 °C and 83–86 °C (Lusas, 2007; Shellhammer & Krochta, 1997), respectively. As these melting point temperatures are significantly higher than the designated drying temperature (20 °C) of the cast emulsion, these waxes have propensity of rapid crystallization when the temperature of the cast emulsion is dropped. The temperature of the cast emulsion was found drop as low as 15 °C at the early stage of drying due to evaporative cooling. The rapid crystallization of these wax seemingly resulted into their random distributed within these films. As these natural waxes were solidified and were embedded within the HAG matrix during the course of drying, the

anticipated preferential migration of wax to film surface did not materialize.

When 10% of these waxes were added to the HAG matrix, the distribution of these waxes within the film matrix were different compared to their respective distribution at 5% concentration (Fig. 5). The presence of 10% of wax in the cast emulsion resulted into the formation of micron scale wax-rich domains in the interior of the dried HAG + wax film, as shown in Fig. 5. In each example where wax is present at 10% in the HAG + wax film, the wax-rich locations showed integrated absorbance values two or more times higher than the base CH₂ absorption values within that sample. For example HAG + 10% CB (Fig. 5) showed a background CH₂ absorbance value of around 3.0 (green shading) while wax rich

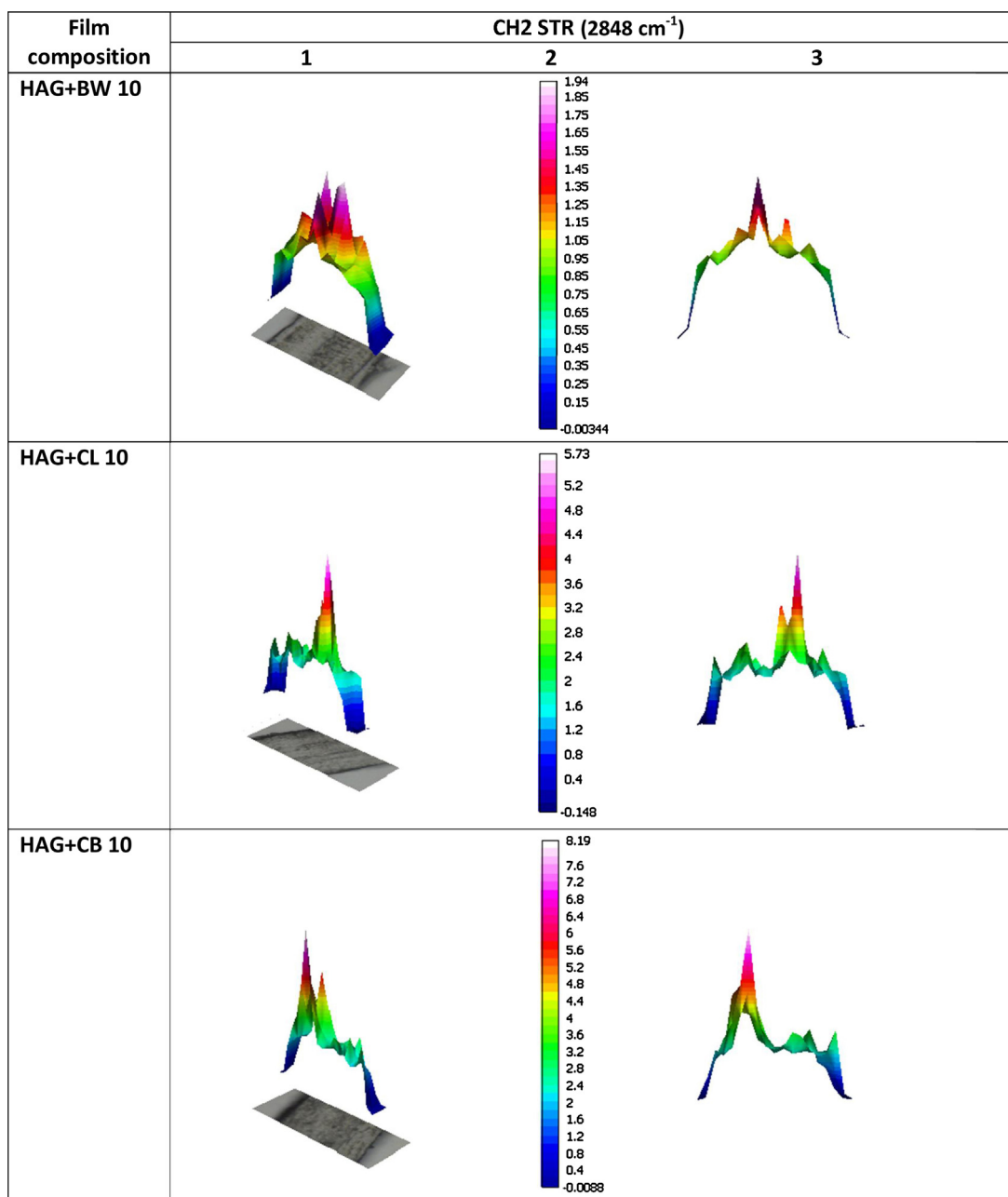


Fig. 5. The functional-group images of wax component within a cross-section of the HAG + 10% wax films. (1) Chemical map with colour codes to indicate presence of wax and/or Tween-80; (2) CH₂ absorbance intensity scale; (3) CH₂ distribution profiles of wax across the thickness of the film. Area under peaks centred at 2848 cm⁻¹ showing CH₂ stretching, lipid distribution and intensity. (For interpretation of the references to colour in this figure legend, the reader is referred to the web version of this article.)

domains show integrated absorbance values of around 7.0 (light pink shading). This observation suggests that if the concentration of wax is higher they tend to form solid wax crystal particles much faster.

It seems that the blending of these waxes at 5% and 10% concentrations into a HAG matrix is unlikely to create a wax-rich (or hydrophobic) layer on the surface of these films. As stated earlier, the natural waxes were found to solidify and crystallize randomly and fairly rapidly due to which their preferential migration to the surface did not appear to occur.

3.2. The distribution of wax in wax + Tween-80 films

The distribution of wax within the HAG + 5% wax + Tween-80 films and HAG + 10% wax + Tween-80 films are illustrated in

Figs. 6 and 7, respectively. The addition of Tween-80 to HAG + wax had altered the wax distribution within these films compared to the distribution of wax within HAG + wax films. At these two concentrations and in the presence of Tween-80 the three natural waxes were found to form wax-rich domain to the interior of the HAG matrix of these films. The presence of both the wax and Tween-80 resulted into confined distribution of wax towards the centre of these films. This distribution can be observed in the CH₂ distribution profile as a domed wax-rich domain in the interior of these films. The CH₂ absorbance intensity scale showed that the concentration of wax progressively decreased towards the surface of these films. Although the wax distribution are similar for all these waxes, the wax-rich location within both of the CB films showed integrated absorbance values displaying higher CH₂ absorption values than the 5% and 10% of BW and CL in the presence of Tween-80. For

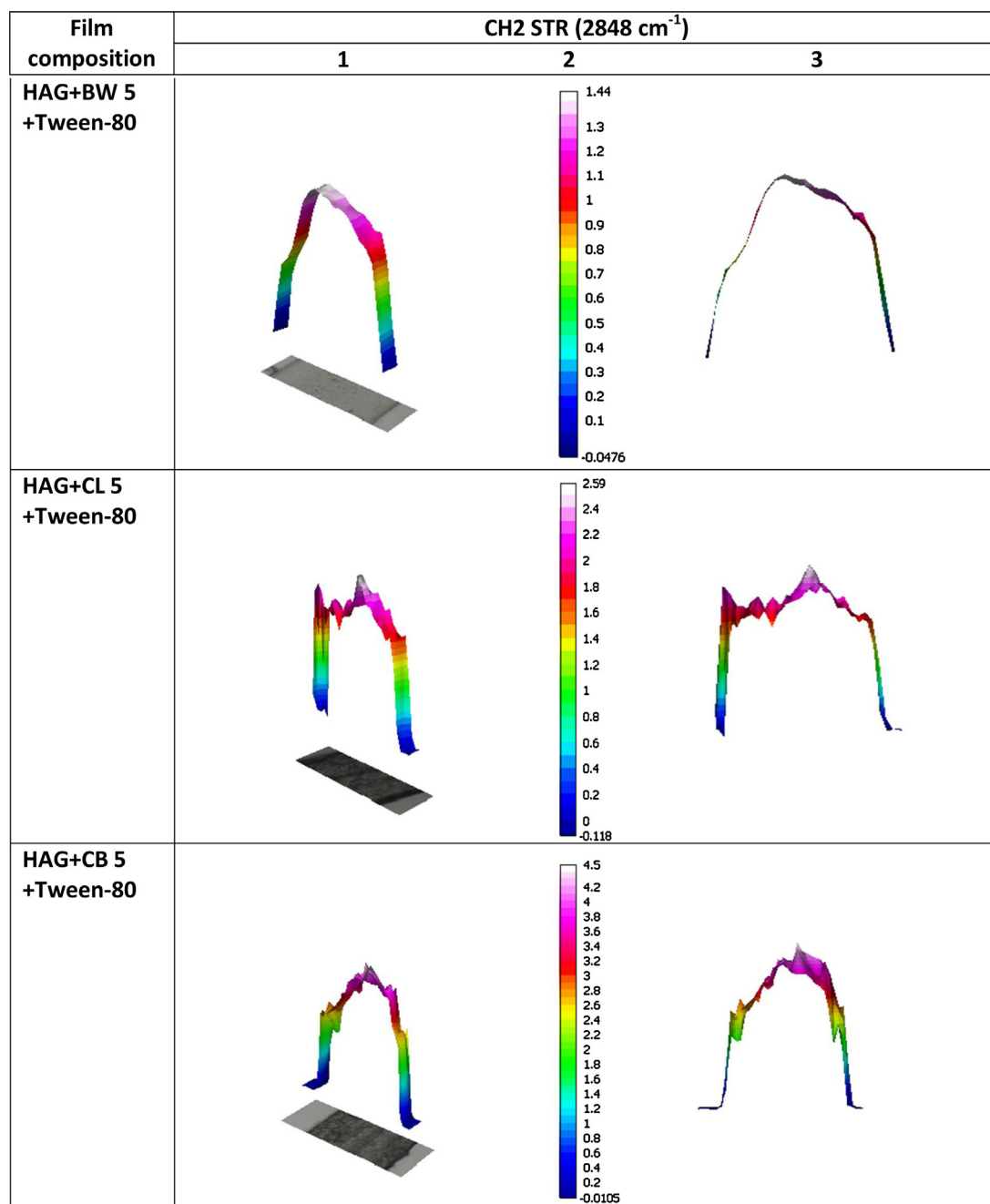


Fig. 6. The functional-group images of wax component within a cross-section of the HAG + 5% wax + Tween-80 films. (1) Map with colour codes to indicate presence of wax and/or Tween-80; (2) CH₂ absorbance scale; (3) CH₂ distribution profiles of wax across the thickness of the film. Area under peaks centred at 2847 cm⁻¹ showing CH₂ stretching, lipid distribution and intensity. (For interpretation of the references to colour in this figure legend, the reader is referred to the web version of this article.)

example HAG + 5% CB + Tween-80 (Fig. 6) showed a wax-rich domain with an integrated absorbance value of 4.5 (light pink shading) while 5% BW and CL displayed lowered integrated absorbance values of 1.44 and 2.59, respectively. This suggests CB is distributed at a higher integrated absorbance value within this film. In Fig. 7, HAG + 10% CB + Tween-80 film had a wax-rich domains with an integrated absorbance value of 10.7 (light pink shading) compared to HAG + 10% CL + Tween-80 film with a value of 4.76 (light pink shading). As seen in Figs. 6 and 7 the films containing 5% and 10% CB + Tween-80 not only exhibited a dome pattern similar to the other waxes, but additionally demonstrated higher integrated absorbance values. These factors could cause the HAG (continuous phase) to be unable to stabilize the emulsion, resulting in wax and Tween-80 phase separation occurred during drying (Perez-Gago &

Krochta, 2005) therefore causing the migration of wax + Tween-80 towards the surface of the films at which the evaporation occurred.

3.3. The distribution of wax and surface hydrophobicity of films

Figs. 4–7 illustrate the chemical maps and integrated absorbance values of HAG + wax and HAG + wax + Tween-80 as stated in Sections 3.1 and 3.2, respectively. The contact angle values of these films are presented in Fig. 8 in order to relate the distribution of wax with film hydrophobicity. The chemical maps of these films and their corresponding contact angle values shed some interesting light on the hydrophobicity of these films.

The contact angle values of these films, whose chemical maps showed that their wax component was either somewhat randomly

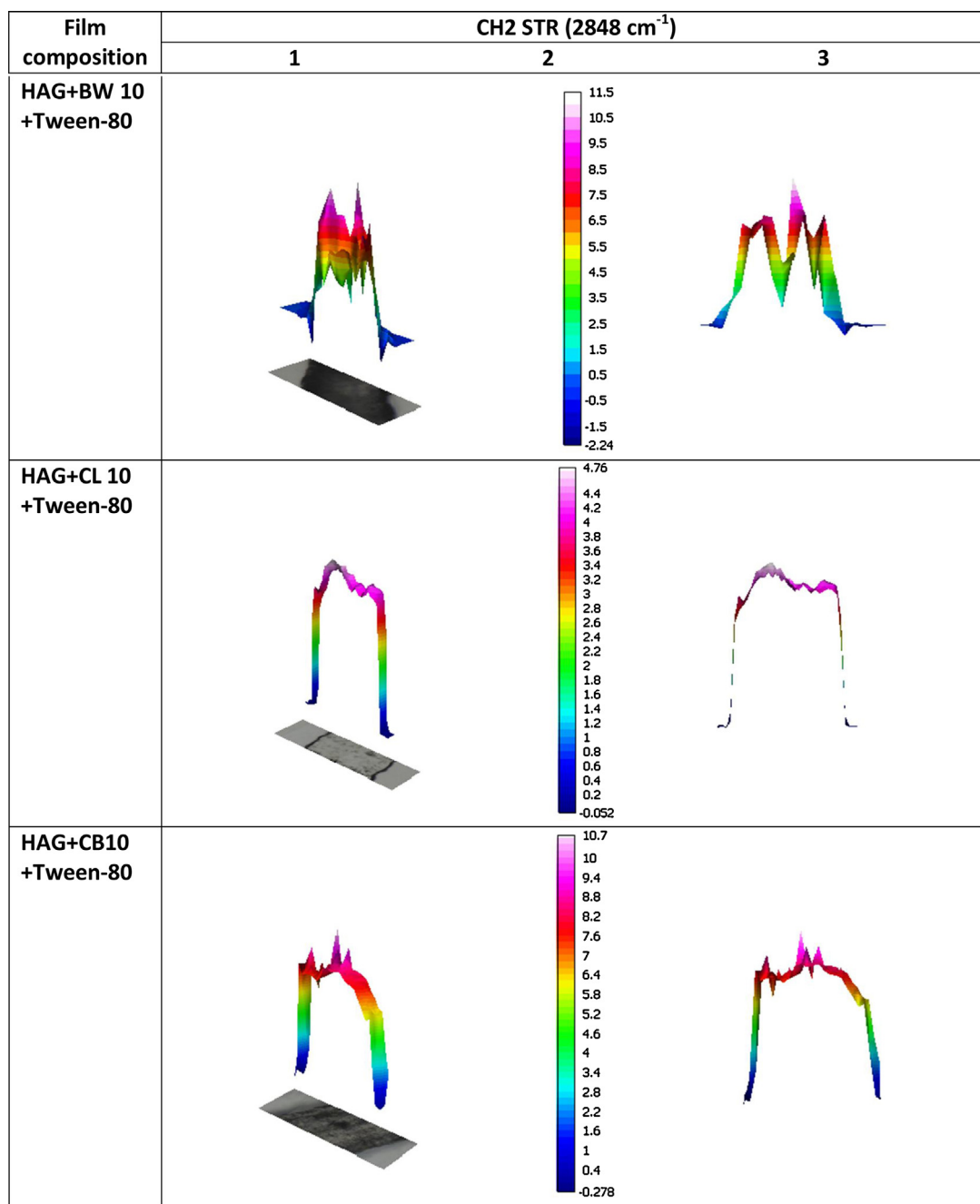


Fig. 7. The functional-group images of wax component within a cross-section of the HAG + 10% wax + Tween-80 films. (1) Chemical map with colour codes to indicate presence of wax and/or Tween-80; (2) CH₂ absorbance intensity scale; (3) CH₂ distribution profiles of wax across the thickness of the film. Area under peaks centred at 2847 cm⁻¹ showing CH₂ stretching, lipid distribution and intensity. (For interpretation of the references to colour in this figure legend, the reader is referred to the web version of this article.)

distributed or remained in the centre region, ranged from 20.7° to 65.6°. The observation of S-FTIR chemical maps presented in Figs. 4–7 explained why such low CA values were obtained in HAG + wax and HAG + wax + Tween-80 films (Fig. 8).

The HAG + BW films at 5% and 10% wax concentrations showed different S-FTIR images. The HAG + 5% BW film showed largely random distribution of BW within the film, whereas the HAG + 10% BW film showed a wax-rich domain in the centre of the film. The contact angle values of the HAG + 5% BW and HAG + 10% BW films were of 44.5° and 65.6°, respectively. It appears that the presence of 5% BW in HAG + 5% BW film does not increase the CA value (compared to the CA of HAG film) ($p > 0.05$) due to the random distribution of the wax in the interior of the HAG matrix. When the concentration

of BW is increased to 10% to the HAG matrix the CA value increased to 65.6°. It can be seen from the S-FTIR map (Fig. 5) that the BW created a wax-rich domain in the interior (towards the centre) of the film. Although the formation of wax-rich domain in the interior of the films is unlikely to increase the contact angle unless a part is protruded to the surface; however, as shown in SEM images of surface morphology (Section 3.4) the formation of wax-rich domains greatly increased the surface roughness of the films. This increased surface roughness seemingly increases the contact angle of the film due to 'Lotus Effect' like phenomenon. The incorporation of CL to HAG matrix had a similar S-FTIR chemical map to those of HAG + BW films. It can be seen from the chemical maps of HAG + 5% CL and HAG + 10% CL (Figs. 4 and 5, respectively) that the distribution of

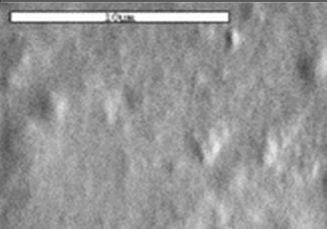
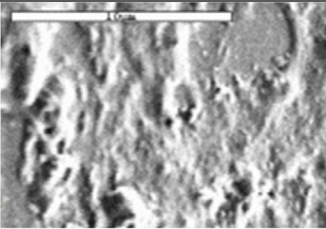
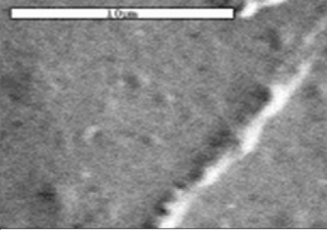
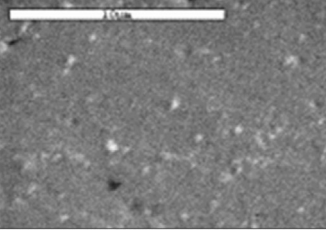
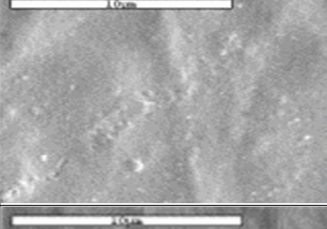
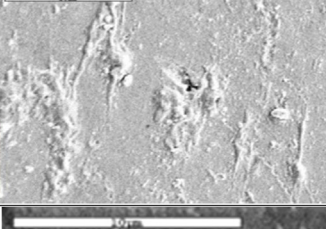
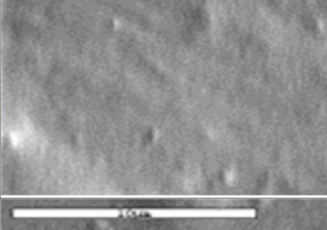
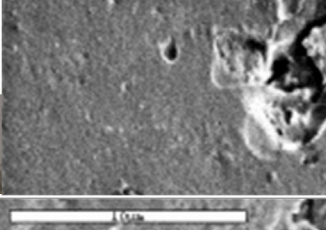
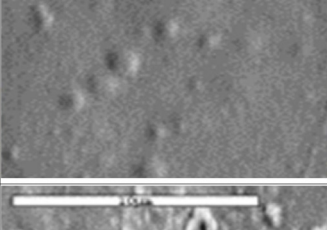
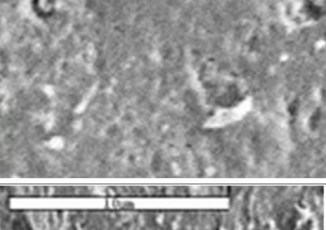
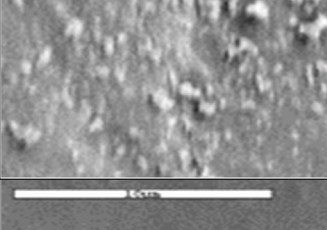
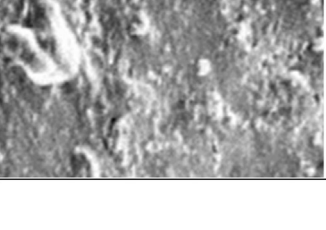
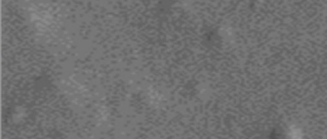
| Composition & CA (°) | SEM | Composition & CA (°) | SEM |
|------------------------------|---|---|---|
| HAG + 5% BW 44.5 ± 1.2 |  | HAG + 5% BW +Tween-80 59.6 ± 1.4 |  |
| HAG + 5% CL 54.5 ± 1.2 |  | HAG + 5% CL +Tween-80 20.7 ± 0.7 |  |
| HAG + 5% CB 48.6 ± 0.7 |  | HAG + 5% CB +Tween-80 87.6 ± 1.3 |  |
| HAG +10% BW 65.6 ± 1.7 |  | HAG +10% BW +Tween-80 55.9 ± 0.8 |  |
| HAG +10% CL 46.5 ± 0.9 |  | HAG +10% CL +Tween-80 41.2 ± 0.5 |  |
| HAG +10% CB 17.8 ± 1.7 |  | HAG +10% CB +Tween-80 80.0 ± 1.7 |  |
| HAG 43.7 ± 1.7 |  | | |

Fig. 8. The SEM images (at 10 μm) and contact angle (CA) values of HAG, HAG + wax and HAG + wax + Tween-80 films (Muscat et al., 2013).

5% CL formed largely random distribution of CL within the film, whereas the HAG + 10% CL showed wax-rich domain within the film. In Fig. 8, the SEM images showed an increase in surface roughness and CA values for the HAG + CL films. The CA values of 54.5° and 46.5° for HAG + 5% CL and HAG + 10% CL, respectively, were significantly higher CA ($p < 0.05$) than the CA value of HAG film. The addition of 5% CB to the HAG matrix displayed a wax-rich domain across the film, as observed in the S-FTIR chemical map (Fig. 4). This rich-wax domain had significantly increased ($p < 0.05$) the CA value compared to that of HAG film. When the concentration of CB in the HAG matrix was increased to 10% this film exhibited signs of starch and wax phase separation during drying (Muscat et al., 2013) causing the CB to form visible droplets on the HAG matrix and displayed a low CA value of 17.8°. This addition of 10% CB to HAG matrix did not form a homogenized film comparable to the other films studied so the CA value of this film will not be included in this study.

The S-FTIR visual maps for the HAG + 5% wax + Tween-80 and HAG + 10% wax + Tween-80 films are presented in Figs. 6 and 7, respectively. The addition of Tween-80 appeared to cause the wax-rich domains to be domed in the interior of these films. Although these waxes had similar wax distribution pattern across the films, the CA values of the HAG + CB + Tween-80 films were significantly higher ($p < 0.05$) at 87.6° and 80.0° (5% CB and 10% CB) compared to 43.7° for HAG film. As discussed in Section 3.2, both these CB + Tween-80 films showed high integrated CH₂ absorption values than 5% and 10% of BW and CL in the presence of Tween-80.

These observations suggest that chemical maps and integrated CH₂ absorption values obtained from S-FTIR can assisted with the hydrophobicity of HAG + wax and HAG + wax + Tween-80 films. The S-FTIR chemical maps; help explain why the incorporation of BW, CL in HAG matrix does not result into segregation of wax towards the surface of the films and fails to increase the surface hydrophobicity in these films. The S-FTIR image maps and integrated CH₂ absorption values also help explain that in the case of CB certain extent of wax segregation occurred on the film surface and hence, greatly increased hydrophobicity.

3.4. The distribution of wax and surface topology of the films

The SEM images for HAG, HAG + wax and HAG + wax + Tween-80 films are shown in Fig. 8. These SEM images illustrate the surface topography of the studied films. As can be seen from these SEM images, the HAG film has a smoother surface compared to other films. The HAG + wax films exhibited rougher surface compared to the HAG film. This rough surface was created by aggregation of wax droplets and subsequent recrystallization during film drying. The S-FTIR visual images help explain the fact that the random distribution of these natural waxes within these films contributed to the increased surface roughness of the HAG + wax films.

The introduction of Tween-80 to the HAG + wax films resulted into different surface topography in these films (Fig. 8). The addition of Tween-80 to HAG + 5% BW, and HAG + 5% and 10% CB had modified the recrystallization of these fat crystals to increase the surface roughness and the CA values of these films. It is apparent the CA value of HAG + 5% BW film increased from 44.5° to 59.6° with the addition of Tween-80 to this matrix. This was also evident with the 5% and 10% CB + Tween-80 films, presenting CA of 87.6° and 80.0°, respectively. The S-FTIR IR absorbance images of these films (Figs. 6 and 7) not only displayed the wax formed a dome pattern within these films but also presented higher integrated absorbance values compared to the other wax + Tween-80 films. Such high integrated absorbance values proved to consequently increase the surface roughness of these films, thus producing higher CA values. Although films HAG + 5% BW + Tween-80 and HAG + CB + Tween-80 exhibited a greater degree of surface roughness compared to

the other wax + Tween-80 films, their CA values vary due to the main constituents present in each wax. Castelli, Uccella, Trombetta, and Saija (1999) reported CB comprised of 12–20% cinnamic and hydroxyl-cinnamic acid esters which are known for their unique hydrophobicity properties. The presence of these esters and Tween-80 in the HAG + CB + Tween films contributed to the higher hydrophobicity of these films. Therefore the combined effect of increase film surface roughness, the highly hydrophobic nature of the CB in the presence of Tween-80 increased the CA value of HAG + CL + Tween-80 films to a hydrophobicity level.

4. Conclusions

The results presented in this study show that S-FTIR could be used to determine the distribution of natural wax and/or Tween-80 within HAG + wax films. The chemical maps generated by the S-FTIR were found to provide information regarding the distribution of waxes within the films. It was found that these waxes were either randomly crystallized within the films at 5% concentration. When 10% of these waxes were added to the HAG matrix, the distribution of these waxes formed wax-rich domains within these films as attained from the S-FTIR chemical maps. The CH₂ absorption value was implemented in providing an understanding of the intensity of each wax within each film and how this relates to the surface hydrophobicity from the SEM images. By utilizing the chemical maps and CH₂ absorption values from S-FTIR, contact angles values and the SEM images one can provide a reasonably link between the distribution of wax, the surface hydrophobicity (contact angle) and surface morphology (topography) of the HAG + wax and HAG + wax + Tween-80 films. From this study it has been showed how a domed wax-rich domain towards the interior of the film, high CH₂ absorption value and increase surface roughness in HAG + 5% and 10% CB + Tween-80 films resulted into a high surface hydrophobicity of 80.0–87.6°, respectively.

Acknowledgements

This work was undertaken on the infrared microspectroscopy beamline at the Australian Synchrotron, Clayton, Victoria, Australia. We thank our colleagues Dr. Huihua Liu and Dr. Amir Ghandi for their assistance with the film window preparation and data collection. This research was supported by Ballarat University led Collaborative Research Network (CRN).

References

- Ali, S. K., Das, U., Lu, Y., Kundapur, V., & May, T. (2011). Chapter 18 – Synchrotron radiation: applications in diagnosis and treatment of malignant brain tumors. In L. Abujamra (Ed.), *Diagnostic techniques and surgical management of brain tumors*. InTech.
- Bourlieu, C., Guillard, V., Vallès-Pamiès, B., & Gontard, G. (2008). Chapter 23: Edible moisture barriers for food product stabilization. In J. M. Aguilera, & P. J. Lillford (Eds.), *Food material science: Principles and practice* (pp. 547–575). Springer.
- Brugnara, M. (2006). *Contact angle plugin*. Trento, Italy: University of Trento. <http://rsbweb.nih.gov/ij/plugins/contact-angle.html> (accessed July, 2012)
- Castelli, F., Uccella, N., Trombetta, D., & Saija, A. (1999). Differences between cumaric and cinnamic acids in membrane permeation as evidenced by time-dependent calorimetry. *Journal of Agriculture and Food Chemistry*, 47, 991–995.
- Coates, J. (2000). Interpretation of infrared spectra – A practical approach. In R. A. Meyers (Ed.), *Encyclopaedia of analytical chemistry*. Chichester: John Wiley and Sons Ltd.
- Dumas, P., Sockalingum, G. D., & Sule'–Suso, J. (2007). Adding synchrotron radiation to infrared microspectroscopy: What's new in biomedical applications? *Trends in Biotechnology*, 25(1), 40–44.
- Han, J. H., & Gennadios, A. (2005). Edible films and coatings: A review. In *Innovations in food packaging. Food science and technology international series*. London: Elsevier.
- Holman, H.-Y., Bjornstad, K. A., McNamara, M. P., Martin, M. C., McKinney, W. R., & Blakely, E. A. (2002). Synchrotron infrared spectromicroscopy as a novel bioanalytical microprobe for individual living cells: Cytotoxicity considerations. *Journal of Biomedical Optics*, 7(3), 417–424.

- Lusas, E. W. (2007). Chapter 34 – Animal and vegetable fats, oils, and waxes. In J. A. Kent (Ed.), *Kent and Riegel's handbook of industry chemistry and biotechnology* (1) (11th ed., 1, pp. 1549–1656). Springer.
- McNaughton, D. (2005). Synchrotron infrared spectroscopy in biology and biochemistry. *Australian Biochemist*, 36(1), 55–58.
- Miller, L. M. (2002). *Infrared microspectroscopy and imaging*. <http://www.bnl.gov/ps/nsls/newsroom/publications/otherpubs/imaging/workshopmiller.pdf>
- Muscat, D., Adhikari, B., Adhikari, R., & Chaudhary, D. S. (2012). Comparative study of film forming behaviour of low and high amylose starches using glycerol and xylitol as plasticizers. *Journal of Food Engineering*, 109, 189–201.
- Muscat, D., Adhikari, R., McKnight, S., Gio, Q., & Adhikari, B. (2013). The physico-chemical characteristics and hydrophobicity of high amylose starch–glycerol films in the presence of three natural waxes. *Journal of Food Engineering*, 119(2), 205–219.
- Park, J. W., Im, S. S., Kim, S. H., & Kim, Y. H. (2000). Biodegradable polymer blends of poly (L-lactic acid) and gelatinized starch. *Polymer Engineering and Science*, 40(12), 2539–2550.
- Perez-Gago, M. B., & Krochta, (2005). Chapter 22: Emulsion and bi-layer edible films. In J. H. Han (Ed.), *Innovations in food packaging* (pp. 384–399). Academic Press.
- Rasband, W. S. (2012). *ImageJ*. Bethesda, USA: U.S. National Institutes of Health. <http://rsb.info.nih.gov/ij/> (accessed July, 2012)
- Rhim, J., & Ng, P. K. W. (2007). Natural biopolymer-based nanocomposite films for packaging applications. *Critical Reviews in Food Science and Nutrition*, 47, 411–433.
- Rhim, J. W., & Shellhammer, T. H. (2005). Chapter 21: Lipid-based edible films and coatings. In J. H. Han (Ed.), *Innovations in food packaging* (pp. 362–380). Academic Press.
- Shellhammer, T. H., & Krochta, J. M. (1997). Whey protein emulsion film performance as affected by lipid type and amount. *Journal of Food Science*, 62(2), 390–394.
- Stuart, B. (2004). *Infrared spectroscopy: Fundamentals and applications*. John Wiley & Sons, Ltd. Chapter 7 – Biological applications.
- Williams, D. L., Kuhn, A. T., Amann, M. A., Hausinger, M. B., Konarik, M. M., & Nesselrode, E. I. (2010). Computerized measurement of contact angles. *Galvanotechnik*, 101(11), 2502–2512.
- Yu, P. (2004). Horizons in nutritional science: Application of advanced synchrotron radiation-based Fourier transform infrared (SR-FTIR) microspectroscopy to animal nutrition and feed science: A novel approach. *British Journal of Nutrition*, 92, 869–885.
- Yu, P. (2012). Board-invited review: Sensitivity and responses of functional groups to feed processing methods on a molecular basis. *Journal of Animal Science and Biotechnology*, 3, 40.
- Zhang, Y., & Han, J. H. (2006). Plasticization of pea starch films with monosaccharides and polyols. *Journal of Food Science*, 71(6), E253–E261.